Combined Experimental and Theoretical Study of the Benzocaine/Ar van der Waals System in Supersonic Expansions

Iker León, Edurne Aguado, Alberto Lesarri,† José A. Fernández,* and Fernando Castaño

Departamento de Química-Física, Facultad de Ciencia y Tecnología, Universidad del País Vasco. Apdo. 644, 48080 Bilbao, Spain

Received: October 2, 2008; Revised Manuscript Received: November 21, 2008

The electronic spectra of Benzocaine·Ar_n, $n = 0-4$ were obtained using two-color resonance enhanced multiphoton ionization; the 1:1 and 1:2 clusters were investigated by ultraviolet/ultraviolet hole burning, stimulated emission pumping, and other laser spectroscopies. A single isomer was found for the 1:1 cluster, while two isomers of the 1:2 cluster were found: one with the two Ar atoms on the same side of the chromophore, and the other with the two Ar atoms sitting on opposite sides of the chromophore. The observed shifts point to the existence of a single isomer for the 1:3 and 1:4 species. Dissociation energies for the neutral ground and first excited electronic state and the ion ground electronic state of the complexes have been determined by the fragmentation threshold method and by ab initio calculations conducted at the MP2 level with 6−31++g(2d, p), 6−311++g(2d, p) and AUG-cc-pVTZ basis sets. The results are compared with those obtained for other similar systems.

I. Introduction

Benzocaine (ethyl-p-aminobenzoate, hereafter, Bz) is a local anesthetic (LA) that has been used for many years in medicine,[1] dentistry, and to adulterate illegal drugs (S-Chart 1of the Supporting Information). Despite that it has been used for a long time, there are still open questions regarding its mechanism of action.[2] The effect of LAs depends on cell membrane potential, channel conformation, pH, and access to the ion-conducting channel. Previously accepted theories on their action mechanisms suggesting a blockage of the ionic channels by the LA have recently been questioned by results from X-rays, which indicate that the molecule is too small to completely block the pore.[3] In addition, site-directed mutagenesis studies[4] have shown that the activity of Bz-type drugs depends specifically on the presence of key amino acids, pointing to a docking mechanism.[5,6] Indeed, a key phenylalanine (F1759 in the human $Na_v1.5$ channel) has been identified as essential for the interaction of the LA with the receptor to take place.[4]

Other studies suggest the existence of direct noncovalent interactions of Bz and other LAs with the lipids of the membrane,[7,8] or even to undesired affinities with proteins, besides those conforming the Na^+ channels, which lead to secondary effects. Thus, a deep knowledge of the LAs noncovalent interactions is necessary if the mechanism of action of such drugs wants to be unraveled. This knowledge is especially valuable to model in silico the molecular mechanisms of the interaction. The huge increase in computing power experienced in the last years allows tackling large-size systems, yielding reliable geometries. However, noncovalent interactions are still hard to model and, very often, the lack of good experimental data hampers the refinement of the theoretical calculations.

Gas phase studies on Bz electronic states and on their noncovalent interactions in microsolvated environments were pioneered by Simons et al.[9−11] and followed by our group.[12−15] A number of van der Waals chromophore/solvent systems, including Bz·Ar were characterized by high resolution LIF ($\sim$0.08 cm^{-1}).[11] In this work, a reinvestigation of the Bz·Ar_n, $n = 1-2$ system is reported, using new powerful spectroscopic mass-resolved techniques. The electronic ground-state geometry of the Bz·Ar_1 complex was already inferred from comparison between the experimental and low level ab initio rotational contours.[11] In this work, we increase knowledge of the system finding a second isomer of Bz·Ar_2 and determining its structure. With the employment of the ion fragmentation threshold method, we estimate the dissociation energies of Bz·Ar_1 and Bz·Ar_2, while the technique of stimulated emission pumping (SEP) provides information on the ground-state vibrational activity. The shifts observed on Bz·Ar_3 and Bz·Ar_4 R2PI spectra give also hints on their structure. Finally, the experimental results are compared with ab initio calculations on the clusters structure, and with results from similar systems.

II. Procedures

A. Experimental. The experimental setup has been described elsewhere[12,16] and only a few details relevant to the present study are summarized below. Bz (Sigma-Aldrich) was heated at 110 °C in an oven and seeded in a buffer gas (either He or a mixture of Ar 5% in He) at 0.5−4 bar stagnation pressure. The mixture was expanded through the 0.5 mm diameter nozzle of a stainless steel pulsed valve (R.M. Jordan) into the vacuum chamber of a time-of-flight mass-spectrometer (TOF−MS, R.M. Jordan) at $<10^{-8}$ bar background pressure. The supersonic expansion freezes the rotational and vibrational degrees of freedom of the complexes to a few K, creating the appropriate conditions to form noncovalent species. The central region of the supersonic beam was skimmed before entering the ionization region of the spectrometer, where the molecules were interrogated by different methods.

* To whom correspondence should be addressed. Departamento de Química-Física, Facultad de Ciencia y Tecnología, Universidad del País Vasco, Apdo. 644, 48080 Bilbao, Spain. Tel: ++ 34 94 601 5387. Fax: ++ 34 94 601 35 00. E-mail:josea.fernandez@ehu.es.

† Present address: Departamento de Química Física y Química Inorgánica, Facultad de Ciencias, Universidad de Valladolid, E-47005 Valladolid, Spain.

10.1021/jp808723r CCC: $40.75
Published on Web 01/20/2009

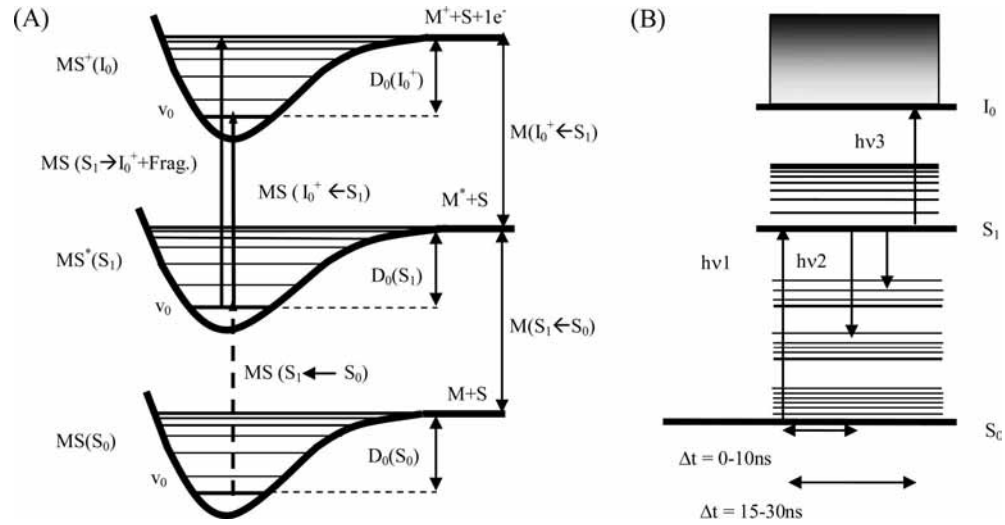

Figure 1. (a) Scheme of the fragmentation threshold method employed to measure dissociation energies. Mass-resolved two-color R2PI transitions are used to derive the potential well depths and dissociation energies of the ground, S_0, first excited, S_1 and ion I_0 ground states. (b) Scheme of the three-laser stimulated emission pumping (SEP); the complex is pumped to the S_1 state with the first laser ($h\nu_1$) and its population probed with the third laser ($h\nu_3$) delayed 15−30 ns. The second laser stimulates the $S_1 \rightarrow S_0$ transition.

Three parallel plates set at 4100, 3750, and 0 V create an electric field that accelerates the ions and send them through the TOF tube (Jordan Inc.) toward the 18 mm diameter multichannel plate detector (MCP, C-0701), where they generate an electrical current. The resulting signal is routed to a digital oscilloscope (Tektronics TDS 520), where it is integrated and transmitted to a PC computer for analysis and storage.

In R2PI spectroscopy, two lasers were directed into the chamber in counter-propagating configuration. The pump laser is tuned to the $S_1 \leftarrow S_0$ transition, whereas a second laser ionizes the molecules. The UV−UV hole burning spectroscopy (HB) was accomplished by probing the sample with a $1 + 1'$ process and monitoring the depletion of the MCP detector signal while scanning the burning laser. The delay between $1 + 1'$ probe and the burning laser is set around $\sim$1 μs. To minimize fragmentation and improve resolution, the hole burning experiments were carried out with three lasers, i.e., using 2-colors for the detection.

The probe laser was a compact Lambda Physics ScanMate dye laser coupled to an in-house Nd:YAG Quantel Brilliant B laser, while a Quantel TDL90 dye laser pumped by a Nd:YAG Quantel YG810 was used as ionization laser. In three laser-experiments, a second ScanMate/Brilliant coupled laser was added. Dye laser wavelengths were calibrated with a Coherent Wavemaster, accurate to <0.01 nm. Appropriate tunable radiation was accomplished with Rhodamine 575 (543−561 nm), Rhodamine 590 (560−577 nm), Rhodamine 610 (575−600 nm), Rhodamine 610 + Rhodamine 640 (579−640 nm), LDS 698 + DCM (640−685 nm), and LDS 698 (670−695 nm) dyes (Exciton). For energy control of the pump laser in two-color experiments a variable attenuator (Newport M-935−10) was used.

The binding energies of the complexes were determined by the ion fragmentation threshold method (Figure 1a).[17,18] The method provides dissociation energies with good accuracy, as long as the $I_0 \leftarrow S_1$ transition does not involve a large change of geometry, and therefore the bottom of the ion potential energy surface can be reached.

Stimulated emission pumping (SEP)[19,20] was performed following the diagram in Figure 1b. The molecules are prepared in the S_1 state using a photon from the pump laser; a second laser, delayed a few ns, probes the molecules using the $I_0^+ \leftarrow S_1$ transition. Between these two lasers, a depopulation laser is fired; when the frequency of its photons is resonant with an $S_1 \leftarrow S_0$ vibronic transition, the stimulated emission channel opens, decreasing the signal from the probe laser. Scanning the wavelength of the depopulation laser, the vibronic spectrum of the S_0 state is obtained. This experiment can be performed with only two lasers, but the described set up permits an active subtraction of the signal if the dump laser is fired at half the repetition rate of the other two. The result is an improvement in the *s*/*n* ratio, since the baseline is less affected by changes in the ionization cross-section.

B. Theoretical Calculations. Ab initio calculations were conducted with the Gaussian 03 suite of programs on an Opteron-based cluster. Some difficulties appeared during the optimization of the system to a true minimum, due to the shallow well of the intermolecular potential energy surface (PES). In some cases, only by selecting strict convergence criteria together with the "opt=CalcAll" option was it possible to achieve convergence. In addition, polarization and diffuse functions are required for a quantitative description of the noncovalent interactions. As the Bz/Ar intermolecular forces are dispersive in nature, the DFT methods are not appropriate.[21] Thus the computation is a compromise between accuracy and CPU time. As described above, despite that the system is not very large for today's standards, it represents a very difficult convergence example, and therefore, the optimization was achieved only after many cycles. All of the data reported in this work are ZPE corrected. The basis set superposition error (BSSE) correction was estimated using the Boys and Bernardi algorithm,[22] although for some of the basis sets employed, it largely overestimated the BSSE of the $Bz \cdot Ar_n$ complexes, yielding corrections close to or even larger than the binding energy, while by definition, the BSSE cannot be larger than the binding energy. Therefore, the largest affordable basis set had to be used in order to minimize the BSSE. Optimizations were carried out using MP2 with three basis sets, namely 6−31 g(d) (for the sake of brevity, the results obtained with the 6–31 g(d) basis set are omitted), 6−31+g(d), and 6−31++g(2d,p), and two final "single point" calculations were carried out on the structures obtained from the MP2/6−31++g(2d,p) calculation, using MP2/6−311++g(2d,p) and MP2/AUG-cc-pVTZ calculation levels. To validate such approximation, *trans*-$Bz \cdot Ar_1$

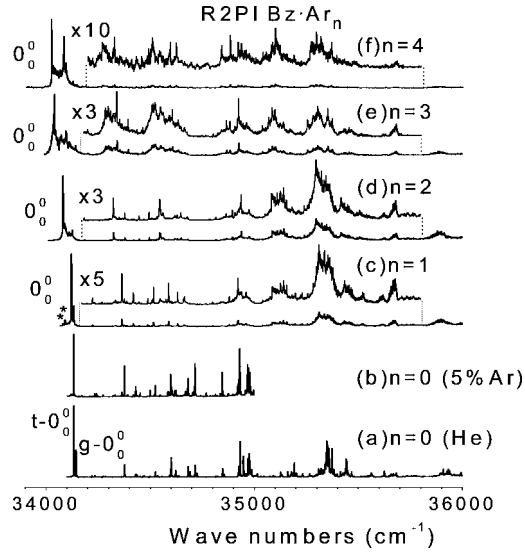

Figure 2. (a) R2PI spectra of bare Bz seeded in He at 0.5−4 barr stagnation pressure and b) in 5% Ar/He mixture at the same stagnation pressure. R2PI spectra of Bz·Ar$_1$ (c), Bz·Ar$_2$ (d), Bz·Ar$_3$ (e), and Bz·Ar$_4$ (f) seeded in 5% Ar/He mixture. In all of the cases, the ionization laser is tuned slightly over the ionization threshold. The peaks marked with an asterisk are due to fragmentation from higher order complexes. A magnified view of spectra (c)−(f) is also offered.

was optimized at the MP2/6−311++g(2d,p), obtaining a structure and a ZPE correction almost identical to those obtained at MP2/6−31++g(2d,p) level.

III. Results

A. Experimental. The R2PI spectra of bare Bz seeded in He (a) and in an 5% Ar/He mixture (b) and of Bz·Ar$_n$ n = 1−4 complexes (c)−(f) are collected in Figure 2. The spectra of Bz in He and Ar and of Bz·Ar$_1$ and Bz·Ar$_2$ complexes in a narrow spectral range have been reported elsewhere,[11−13] and are in good agreement with those obtained here. As pointed out recently,[14] the collisions with Ar have enough energy to transfer the gauche-conformer population to the trans-conformer. In consequence, all of the features observed in Figure 2b are assigned to the *trans*-Bz conformer. In addition, the first ∼400 cm^{-1} of the Bz·Ar spectrum matches those of *trans*-Bz except for a progression developed on the origin band on a low frequency intermolecular mode of ∼11 cm^{-1}, assigned to the intermolecular mode ν_1 (14 cm^{-1} frequency calculated at MP2/6−31++g(2d,p) level, see Table S-1 and Figure S-1of the Supporting Information). Also, the chromophore intramolecular vibrations are weaker compared to its 0_0^0 transition in the Bz·Ar$_1$ R2PI spectrum, than those on the bare Bz spectrum, disappearing around ∼500 cm^{-1}. The rest of the peaks to the blue are associated with fragmentation from the Bz·Ar$_2$ complex. The 12 cm^{-1} shift between the Bz·Ar$_1$ and Bz 0_0^0 bands suggests a small influence of the electronic excitation on the binding energy.

The Bz·Ar$_2$ spectrum shows a substantial vibrational activity near the origin, which we tentatively assign to the red-most peak, at 34081 cm^{-1}. A number of features due to intermolecular vibrations add up to form a broad absorption of ∼60 cm^{-1}, on top of which several peaks and shoulders can be distinguished. As it will be demonstrated bellow by hole burning spectroscopy, one of the peaks is the origin of a second isomer, namely Isomer 2. As in the lowest ∼+500 cm^{-1} region of the Bz·Ar$_1$, the intensity of the vibrational bands compared to that of the 0_0^0 band is smaller than for Bz. The spectrum extends up to ∼2200 cm^{-1}, but it is not feasible to discriminate the Bz·Ar$_2$ bands from the Bz·Ar$_3$ fragmentation, and therefore, it is not possible to determine the real extension of the 1:2 spectrum.

TABLE 1: Ionization and Fragmentation Energies and Origin Band Shifts Relative to the Bare Bz 0_0^0 Transition (values are in cm^{-1})

	$S_1 \leftarrow S_0$	shift	$I_0^+ \leftarrow S_1$	fragment $\leftarrow S_1$
t-Bz	34134	0	28981	
g-Bz	34145	11	28991	
$BzAr_1$	34122	−12	28917	29416
$BzAr_2$-Isomer 1	34081	−53	28859	29442 (2→1)
				30016 (2→0)
$BzAr_2$-Isomer 2	34110	−24		
$BzAr_3$	34041	−93		
$BzAr_4$	34027	−107		

The spectra of Bz·Ar$_3$ and Bz·Ar$_4$ complexes have similar overall appearance: a quasi-continuum with no discrete features. The peak at 34041 cm^{-1} is assigned to the Bz·Ar$_3$ 0_0^0 band, which is then shifted ∼40 cm^{-1} with respect to that of Bz·Ar$_2$. Another peak at 34 095 cm^{-1} could be the origin of a second isomer or a particularly strong intermolecular vibration.

The spectrum of Bz·Ar$_4$ has at least two peaks that may be identified as its origin band: the stronger one at 34 027 cm^{-1} and the other at 34 085 cm^{-1}. On the basis of the relative shifts of the complexes studied, we assign the stronger red-shifted peak to the Bz·Ar$_4$ 0_0^0 band, i.e., shifted ∼107 cm^{-1} from the Bz 0_0^0 transition, being the partner peak due either to fragmentation from higher order complexes, to an hypothetical second conformer or to a particularly intense vibrational mode.

Table 1 collects the position of the origin bands of the spectra depicted in Figure 2. The shift of the 0_0^0 transition of Bz·Ar$_2$ Isomer 1 relative to that of Bz·Ar$_1$ is −41 cm^{-1}, which is considerably larger than the Bz → aBz·Ar$_1$ shift, indicating that in this isomer the second Ar is not placed symmetrically relative to the first one, and therefore, both Ar atoms are on the same side of the ring. Moreover, the origin of isomer 2 is shifted 24 cm^{-1}, i. e., twice the shift found for the 1:1 complex, pointing to a sandwich structure. In the same way, the 1:4 → 1:0 shift is twice the 1:2 → 1:0 Isomer 1 shift and therefore, following the additively rule, very likely the 1:4 cluster has two Ar atoms on each side of the aromatic ring.

Figure 3 depicts the ionization and fragmentation onsets of *trans*- and *gauche*-Bz, Bz·Ar$_1$, and Bz·Ar$_2$ Isomer 1. Unfor-

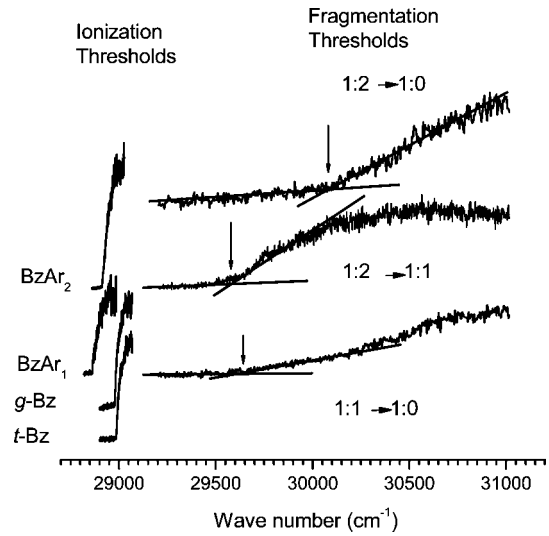

Figure 3. Ionization and fragmentation thresholds of *trans*-Bz, *gauche*-Bz, Bz·Ar$_1$, and Bz·Ar$_2$ Isomer 1.

TABLE 2: Binding Energies of the Bz·Ar$_1$ and Bz·Ar$_2$ Complexes, As Obtained from the Fragmentation Threshold and from Calculations[a]

	binding energy determination method						
	fragmentation threshold			calculation (S_0) MP2			
	S_0	S_1	I_0^+	6−31+g(d)	6−31++G(2d,p)	6−311++G(2d,p)	Aug-cc-pVTZ
$BzAr_1$	423	435	499	776 (trans)	664 (296)	618 (343)	772 (540)
				836	*398*	*275*	*232*
				1016 (gauche)	742 (402)	677 (303)	660 (430)
				853	*340*	*374*	*230*
$BzAr_2$	484[b]	525[b]	583[b]	1606[d]	1424[d] (640)	1264[d] (713)	1528[d] (1100)
	982[c]	1035[c]	1157[c]	*1688*	*784*	*551*	*428*
				1762[e]	1456[e] (797)	1310[e] (736)	1644[e] (1194)
				1762	*659*	*574*	*450*

[a] The energies are in cm^{-1}. Values in parentheses are BSSE corrected. Values in cursive are the BSSE estimation using the Boys and Bernadi counterpoise method. [b] Evaporation of the first Ar atom. [c] Evaporation of both Ar atoms. [d] Isomer with both Ar atoms on the same side. [e] Isomer with the Ar atoms on different sides of the chromophore.

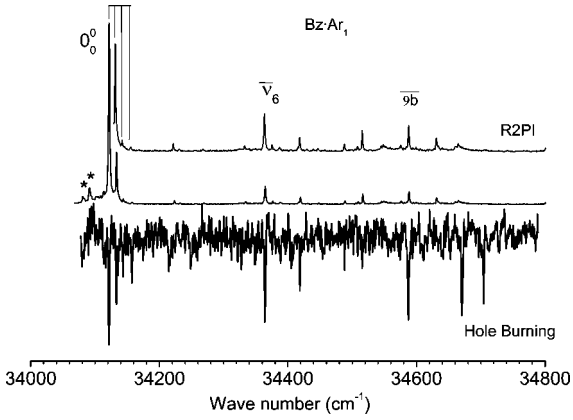

Figure 4. UV−UV hole burning spectrum of the $BzAr_1$ complex. The R2PI spectrum is also shown for comparison. Assignments are taken from ref 13. The peaks marked with asterisks are due to fragmentation from higher order clusters.

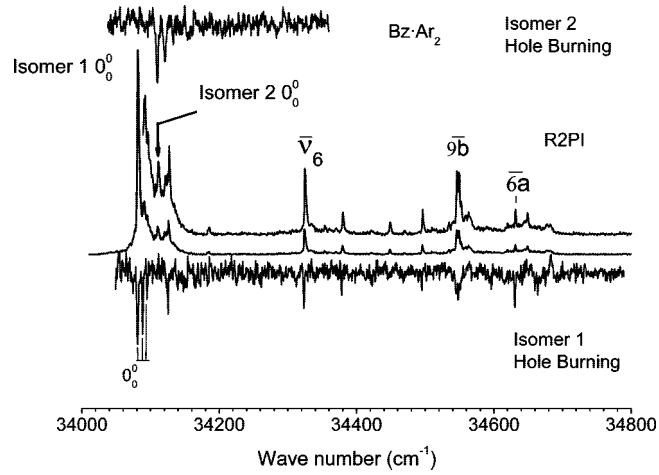

Figure 5. UV−UV hole burning and R2PI spectra of $BzAr_2$ complex. The R2PI spectrum is shown for comparison purposes. Two isomers are identified. Ball and stick representations of the active intermolecular modes can be found in the Supporting Information.

tunately, due to the low *s*/*n* ratio, it was not possible to carry out the same experiments for the rest of the species. The binding energies estimated for the complexes using the fragmentation threshold method are collected in Table 2. The shift on the $I_0 \leftarrow S_1$ transition between the Bz conformers is 10 cm^{-1}, in good agreement with the values reported elsewhere.[13] These ionization onsets are affected by the extraction field of the ionization region of the spectrometer, shifting the energy some ∼100−200 cm^{-1} and thus they should be taken as lower limits.[14]

The comparison between the R2PI spectra in Figure 2 suggests the presence of a single isomer of Bz·Ar$_1$ and two isomers of the 1:2 complex. Further confirmation is obtained from the hole burning spectra shown in Figures 4 and 5. All major features in the R2PI spectrum of the 1:1 complex (Figure 4) are mirrored in the corresponding hole burning spectrum, confirming the existence of a single isomer. The peaks to the red of the Bz·Ar$_1$ 0_0^0 band, assigned to Bz·Ar$_2$ fragments are missing in the *hole burning* trace, as expected. However, the hole burning traces obtained for the 1:2 complex demonstrate the existence of at least two conformers, with origin bands shifted −41 and −12 cm^{-1}, respectively, from the 1:1 0_0^0 transition. The broad absorption on the first ∼60 cm^{-1} to the blue of the Bz·Ar$_2$ 0_0^0 transition is well resolved in the hole burning trace, allowing the observation of a progression of 3 member separated 7 cm^{-1}, built on the origin of Isomer 1, which matches very well the $\bar{\nu}_1$ intermolecular mode depicted in Figure S-2 of the Supporting Information, in which the two Ar atoms move in opposite directions over the aromatic ring ($\bar{\nu}_1$= 5 cm^{-1} at MP2/6−31++g(2d,p) calculation level, see Table S-1of the Supporting Information). Another peak at 46 cm^{-1} from Isomer 1 0_0^0 transition is assigned to the $\bar{\nu}_5$ intermolecular mode, which is strongly coupled to the torsion of the Ph-COOEt bond, with a calculated frequency of 45 cm^{-1} at the MP2/6−31++g(2d,p) level (Figure S-2 of the Supporting Information). A progression of 13 cm^{-1} is also observed on Isomer 2, which could be assigned either to $\bar{\nu}_1$= 10 cm^{-1} or $\bar{\nu}_2$ = 11 cm^{-1} (see Figure S-3 of the Supporting Information for a ball and stick representation of both vibrations).

Figures 6−8 show the SEP spectra of Bz, Bz·Ar$_1$ and of Bz·Ar$_2$ Isomer 1, along with their R2PI spectra, while the bands positions are collected in Table S-2 of the Supporting Information. A comparison between the SEP and the R2PI spectra of bare Bz (Figure 6) shows a shift on the vibrations' wavelengths between ground and excited electronic states. In addition, a few bands vary their relative intensities. The 0_0^0 band appears as a positive peak because when the depletion laser frequency is resonant with this transition, the signal increases. However, the SEP transitions appear as negative peaks. The SEP is in good agreement with the dispersion emission spectra of the bare Bz reported elsewhere.[13] Note the lack of bands in the SEP spectrum below ∼400 cm^{-1} as the first band appears at 423 cm^{-1}. The rest of the spectra have a rich spectroscopy, until the last band observed at 1750 cm^{-1}. Actually, the calculations show that there is a vibrationless gap between the normal modes ν_{52} = 1750 cm^{-1} (C=O stretching) and ν_{53} = 3109 cm^{-1} (a vibration of the ethyl group), in good agreement with the experimental

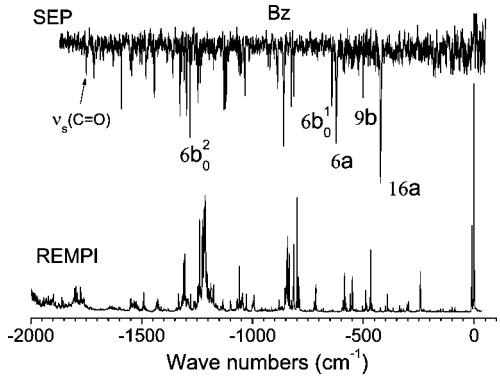

Figure 6. Stimulated emission pumping spectrum of benzocaine. The R2PI spectrum is also included for comparison. The bands positions are collected in Table S-2 of the Supporting Information, while the calculated normal modes are collected in Table S-1 of the Supporting Information. Note that the REMPI trace is mirrored to easy the comparison and that its *x* scale should run positive.

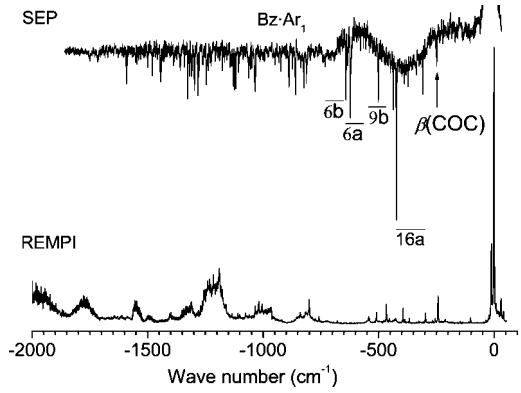

Figure 7. Comparison between the stimulated emission pumping (SEP) and the R2PI spectra of the $BzAr_1$ complex. The band's positions are collected in Table S-2 of the Supporting Information, while the calculated normal modes are collected in Table S-1 of the Supporting Information. Note that the REMPI trace is mirrored to easy the comparison and that its *x* scale should run positive.

data. Some other bands the calculated data match very well, although a complete assignment was not attempted, due to the large number of vibrational modes. However, it is not possible to establish a clear correspondence between the REMPI and SEP bands or between the REMPI spectrum and the calculated normal modes, because of their large number and the shifts between ground and excited states. In addition, one must keep in mind that SEP is a 2-photon process to the ground electronic state, while REMPI involves in the first resonance step only one photon to the excited electronic state. So even if the vibrational structure in ground and electronic state are identical the SEP and REMPI spectra will be different because they probe different sets of levels because of the selection rules. The detailed list of bands on the spectra of Figures 6−8, can be found in Table S-2 of the Supporting Information, while the calculated normal modes are in Table S-1 of the Supporting Information.

Figure 7 depicts the SEP and R2PI spectra of the $Bz\cdot Ar_1$ complex. The lowest frequency band observed is at 246 cm^{-1}, which could be assigned to $\nu_9 = 246$ cm^{-1} (COC bending mode). There is a fluctuation on the baseline up to ∼600 cm^{-1}, when it becomes constant for the rest of the spectrum. The origin of this fluctuation is not clear, as it is not present on the bare molecule SEP spectrum. One possibility is the presence of intermolecular vibrations that are not seen in the REMPI experiment, but additional experiments should be performed to

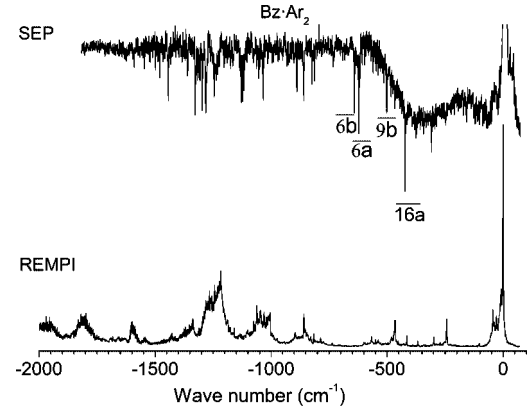

Figure 8. Comparison between the stimulated emission pumping and the R2PI spectra of the $BzAr_2$ Isomer 2. The band's positions are collected in Table S-2 of the Supporting Information, while the calculated normal modes are collected in Table S-1 of the Supporting Information. Note that the REMPI trace is mirrored to easy the comparison and that its *x* scale should run positive.

clarify this point. Well-resolved transitions are observed up to ∼1500 cm^{-1} where the band intensities decrease until they finally disappear. The SEP technique permits one to separate the spectrum of the 1:1 complex from the fragmentation, resulting in a spectrum with well-resolved transitions. However, no intermolecular transitions are observed in the SEP spectrum, probably due to its low intensity. As already mentioned above, only a weak intermolecular mode is active in the R2PI spectrum. However, several intramolecular bands not observed in the chromophore SEP gain intensity in the complex. Both Bz and $Bz\cdot Ar_1$ SEP spectra match very well beyond −500 cm^{-1}, except for a decrease in the intensity of the $BzAr_1$ bands around ∼−1500 cm^{-1} that finally disappear below −1700 cm^{-1}.

A comparison between the SEP and R2PI spectra of $Bz\cdot Ar_2$ is presented in Figure 8. The SEP spectrum is similar to that of $Bz\cdot Ar_1$ (Cf. Figure 7): in the first ∼600 cm^{-1} both have a broad emission, whose origin is not clear. From the broad emission, a few vibronic transitions emerge that match those observed in the 1:1 spectrum. Beyond ∼−590 cm^{-1} from the 0_0^0 transition, the background disappears and with small changes, the same vibronic lines as for the $Bz\cdot Ar_1$ are observed, assigned to intramolecular modes. The peak intensities weaken beyond ∼−1400 cm^{-1} and disappear near ∼−1600 cm^{-1}.

B. Calculations. Table 2 shows the dissociation energies for all of the structures calculated, together with the BSSE estimated using the counterpoise method. As can be seen, the method yields a BSSE of ∼800 cm^{-1} for the 1:1 complex at the MP2/6−31+G(d) level, which is of the same order of magnitude as the binding energy at that calculation level. Increasing the basis set, the BSSE decreases, as expected, but even for the largest basis set employed, the counterpoise method yields an estimation for the BSSE around the 30% of the uncorrected dissociation energy.

The structures of $Bz\cdot Ar_1$ and $Bz\cdot Ar_2$ complexes computed at MP2/6−31++g(2d,p) are displayed in Figure 9, whereas Table 3 collects the rotational constants obtained from such structures, together with the experimental values from ref 11. A good agreement between both sets of values is observed, which demonstrates that the calculation level employed is high enough to accurately describe the cluster structures. The reliability of the calculated structures is also demonstrated by the good agreement between experimental vibronic frequencies and calculated normal modes, as pointed out earlier.

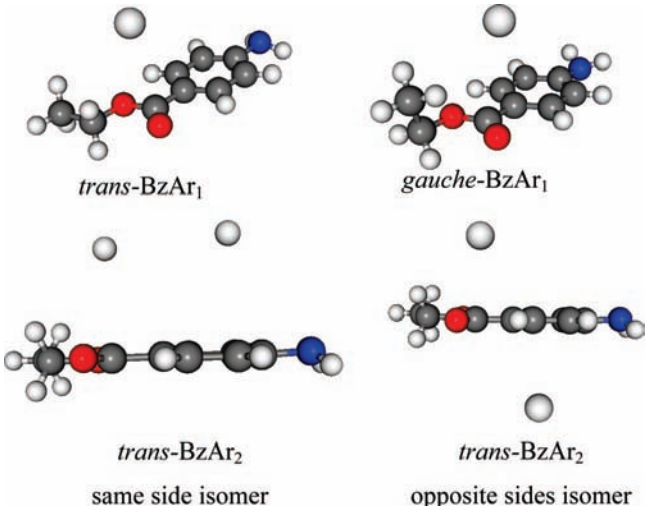

Figure 9. Structures of $BzAr_1$ and $BzAr_2$ complexes calculated at MP2/6−31++g(2d,p) level. The normal modes are listed in Table S-1 of the Supporting Information, while the intermolecular modes are depicted in S-Figures 1−3 of the Supporting Information.

TABLE 3: Comparison between Computed and Experimental Rotational Constants

	rotational constants (cm^{-1})					
	A		B		C	
	exp.	calc.	exp.	calc.	exp.	calc.
t-Bz	0.08131	0.0844	0.01467	0.0147	0.01249	0.0126
g-Bz	0.09237	0.0963	0.01424	0.0146	0.01277	0.0132
t-$BzAr_1$	0.03509	0.0323	0.01113	0.0119	0.01002	0.0109
g-$BzAr_1$		0.0330		0.0130		0.0112
t-$BzAr_2$ SS		0.0209		0.0103		0.0082
t-$BzAr_2$ OS		0.0187		0.0101		0.0077

[a] Calculated values obtained at the MP2/6-31++g(2d, p) level. Experimental values from refs 10 and 11.

The $Bz\cdot Ar_2$ structures based on *trans*-Bz have been explored, finding two isomers: one with the two argon atoms sitting on the same side of the chromophore and another one with one atom on each side. In the former, there is an additional contribution due to the Ar−Ar interaction, but the second Ar atom enters in a less favorable position. As a result, the difference in the stability between both isomers is well within the calculation error, and therefore one would expect to find both isomers in the expansion.

IV. Discussion

Structure of the Complexes. The geometry of the $Bz\cdot Ar_1$ cluster proposed by Simons et al.[11] from comparison between high resolution LIF and rotational contour simulations is built upon the *trans*-Bz conformer with the Ar atom sitting over the aromatic ring. The evidence reported in this work confirms such assignment. Although the comparison between experimental and calculated rotational constants alone does not allow us to perform an univocal assignment, the similarity between the *trans*-Bz and $Bz\cdot Ar_1$ spectra constitute a strong evidence in favor of such assignment.

The two calculated isomers for the 1:1 complex have similar stability, and therefore, one would expect to have both in the supersonic expansion. However, the collisions with Ar provide enough energy to trigger the isomerization process, pumping the population from the gauche species to the more stable trans-conformer.[14] Consequently, the complexes derived from the *gauche*-Bz conformer are not observed.

Two isomers are found experimentally for the 1:2 complex; the 0_0^0 band of Isomer 1 presents a shift of 41 cm^{-1} with respect to that of $Bz\cdot Ar_1$, while Isomer 2 exhibits a 12 cm^{-1} shift relative to the 1:1, which is identical to the 1:1 → 1:0 0_0^0 shift, suggesting that the second Ar atom enters in a position equivalent to that of the first one. Therefore, we assign the origin band at 34110 cm^{-1} (Isomer 2) to the $Bz\cdot Ar_2$ complex with the two Ar on opposite sides of the chromophore (OS isomer in Figure 9). Consequently, Isomer 1 is assigned to the structure labeled as SS in Figure 9, which has the two Ar atoms on the same side of the chromophore.

The first Ar that attaches to the chromophore interacts with the esther group, and therefore, it is not affected much by the electronic excitation, resulting in a mere 12 cm^{-1} shift on the 0_0^0 transition. If the second Ar atom enters in the opposite side of the chromophore, then the 0_0^0 band shifts another 12 cm^{-1}. However, when the second Ar enters in the same side of the chromophore (Isomer 1), it interacts with the aromatic ring. Such interaction is more affected by the electronic excitation, and therefore, this isomer presents a longer 0_0^0 transition shift. Certainly, the observed shift for this isomer (−53 cm^{-1} relative to the bare molecule) is identical to the one observed for aniline·Ar, where the Ar atom interacts directly with the aromatic ring.[23]

The 0_0^0 transition of the 1:3 cluster is shifted ∼−93 cm^{-1} with respect to the bare molecule, and ∼40 cm^{-1} from the 1:2 Isomer 1, suggesting that the third Ar atom is interacting with the ring. So, very likely, the 1:3 complex has the three Ar atoms on the same side of the chromophore. However, the origin band of the 1:4 cluster is shifted ∼−107 cm^{-1} from the bare molecule 0_0^0 transition, i.e., twice the shift observed for the 1:2 Isomer 1, and therefore, the two additional Ar atoms of the 1:4 cluster occupy positions equivalent to those occupied by the Ar atoms of the 1:2 complex. As a consequence, $Bz\cdot Ar_4$ is expected to have two Ar atoms on each side of the ring.

There are another peaks in the 1:3 and 1:4 spectra that may be assigned to secondary isomers. Unfortunately, the unfavorable *s/n* ratio hampers to obtain the hole burning spectra. In addition, the observed shifts of those peaks does not give a clear hint on the assignment: they are shifted 55 and 58 cm^{-1} from the 1:3 and 1:4 0_0^0 transitions, respectively. Although they may be due to a second isomer of each stoichiometry, one cannot discard the assignment to a particularly strong intermolecular vibration.

Binding Energies. An attempt to experimentally determine the cluster's dissociation energy was made using the fragmentation threshold method. As described in the Introduction, this method works reasonably well if the Franck−Condon window allows access of the bottom of the ion ground electronic state well. Table 2 collects the values obtained by this method together with those obtained from the calculations. As can be seen, the experimental values obtained for the 1:1 species are bracketed between those obtained with 6−311++g(2d,p) and AUG-cc-pVTZ basis sets.

Other aromatic-Ar systems have binding energies of the same order as $Bz\cdot Ar_1$. For example, Fajin et al.[24] reported an S_0 dissociation energy of 425 cm^{-1} for fluorobenzene/Ar, computed at CCSD(T) level with the AUG-cc-pVDZ basis set augmented with 3s3p2d1f1g midbond functions. Also, Ishiuchi et al.[25] determined a dissociation energy of 359 cm^{-1} for Phenol/Ar from fragmentation in the REMPI spectrum. Both systems are expected to have lower interaction energies than $Bz\cdot Ar_1$ because of their smaller size. Furthermore, the Ar atom in the $BzAr_1$ complex sits over the ester group, instead of on the aromatic ring as in the fluorobenzene and phenol complexes. The Ar/

ester group interaction is therefore stronger than the Ar/aromatic ring and consequently, Bz·Ar_1 is expected to have a higher interaction energy.

In aniline·Ar, Gu et al.[23] determined a dissociation energy of 380 ± 15 cm^{-1} for S_0, 440 ± 15 cm^{-1} for S_1 and 495 ± 15 cm^{-1} for the ion 1:1 complex using MATI. As can be seen, the Bz·Ar_1 dissociation energy is ∼10% larger in S_0, but its D_0^+ dissociation energy is almost identical to the aniline·Ar D_0^+ dissociation energy. The interaction with the positive charge dominates in the ion, and it is similar for both aniline·Ar_1 and Bz·Ar_1. The fragmentation threshold method employed in this work is less accurate than the MATI method used in ref 23. In addition, it is difficult to estimate the error bars of the data obtained by the fragmentation threshold, as the main source of error is the accessibility of the bottom of the ion PES. Therefore, the excellent agreement between the data in ref 23 and those in Table 2 validates our results.

Gu et al. also determined the dissociation energy of aniline·Ar_2,[23] reporting a value of 1020 ± 20 cm^{-1} for the evaporation of both Ar atoms in D_0^+. Such a value is also very similar to the one of 1157 cm^{-1} (see Table 2) obtained in this work, taking into account that the structure of the aniline·Ar_1 cluster analyzed in ref 23 has the two Ar placed symmetrically on opposite sides of the chromophore (isomer (1|1) according to their nomenclature), while the experimental data in Table 2 are for the Bz·Ar_2 Isomer 1, with both Ar's on the same side of the chromophore (isomer (2|0) according to their nomenclature). Nevertheless, as the data in Table 2 show, both Bz·Ar_2 isomers have very similar dissociation energies.

The comparison between the experimental and calculated binding energies show that the experimental values are bracketed between those obtained at the MP2/6−311++g(2d,p) level and the ones obtained at MP2/AUG-cc-pVTZ. Both sets of data show a moderated agreement with the experimental values. However, the good agreement between experimental and calculated rotational constants and between the band positions and the calculated normal modes confirms that an adequate calculation level was employed for the description of the experimental structure. The main source of error stems from the estimation of the BSSE using the counterpoise method. There is no other alternative but to further increase the basis sets employed, in order to reduce the BSSE. Even so doing, it is not clear that a convergence to the correct value will be achieved. This reinforces the necessity for obtaining experimental data on systems formed by noncovalent interactions, to further refine the calculation procedures.

V. Conclusions

Bz·Ar_n, $n = 1-4$ complexes have been studied by 2-color R2PI, mass-resolved hole burning, SEP and ab initio calculations. The hole burning experiments allow one to identify a single isomer for the 1:1 complex, and two isomers for the 1:2 complex, all of which having the chromophore in the trans conformation. The stronger 1:2 isomer is assigned to the calculated structure in which both Ar's are on the same side of the chromophore, whereas the weaker isomer corresponds to a structure with the Ar atoms placed symmetrically on opposite sides of the chromophore. The observed spectral shifts point to a structure with the 3 Ar atoms on the same side of the chromophore for the 1:3 cluster and to a symmetric structure with 2 Ar atoms on each side of the ring for the 1:4. Binding energies were obtained by ab initio calculations and the fragmentation threshold method. The calculations yield binding energies of ∼440 ± 100 cm^{-1} and 900 ± 200 cm^{-1} for the 1:1 and 1:2 species, respectively, while the fragmentation threshold method yields values of 423, 435, and 499 cm^{-1} for the 1:1 complex in S_0, S_1, and D_0^+ electronic states, and of 982, 1035, and 1157 cm^{-1} for the 1:2 complex with both Ar atoms on the same side of the chromophore in S_0, S_1, and D_0^+ electronic states, respectively. The results are in good agreement with those obtained for similar systems, especially when compared with previous works on aniline·Ar.

Acknowledgment. This work was partially supported by MEC (Madrid, Spain) under Grant CTQ2003-0510 and Consolider Grant CSD2007-00013), the Basque Government, and the UPV under Consolidated Group Grants over the last years. The SGIker UPV/EHU Facilities, supported by the European Social Funding and MCYT, are acknowledged for computational resources. I.L. thanks the GV for an undergraduate fellowship.

Supporting Information Available: Supporting figures and tables as described in the text. This material is available free of charge via the Internet at http://pubs.acs.org

References and Notes

(1) Berde, C. B.; Strichartz, G. R.; Miller, R. D. Local Anesthetics. In *Anesthesia*; Miller, R. D., Ed.; Churchill Livingstone: New York, 2004.
(2) Scheuer, T. *J. Physiol.* **2007**, *581*, 423.
(3) Jiang, Q. X.; Wang, D. N.; MacKinnon, R. *Nature* **2004**, *430*, 806.
(4) Ragsdale, D. S.; Mcphee, J. C.; Scheuer, T.; Catterall, W. A. *Science* **1994**, *265*, 1724.
(5) Wang, G. K.; Wang, S. Y. *J. Gen. Physiol.* **1994**, *103*, 501.
(6) Wang, S. Y.; Mitchell, J.; Moczydlowski, E.; Wang, G. K. *J. Gen. Physiol.* **2004**, *124*, 691.
(7) Kuroda, Y.; Nasu, H.; Fujiwara, Y.; Nakagawa, T. *J. Membr. Biol.* **2000**, *177*, 117.
(8) Shibata, A.; Maeda, K.; Ikema, H.; Ueno, S.; Suezaki, Y.; Liu, S.; Baba, Y.; Ueda, I. *Colloids Surf., B* **2005**, *42*, 197.
(9) Howells, B. D.; McCombie, J.; Palmer, T. F.; Simons, J. P.; Walters, A. *J. Chem. Soc., Faraday Trans.* **1992**, *88*, 2587.
(10) Howells, B. D.; McCombie, J.; Palmer, T. F.; Simons, J. P.; Walters, A. *J. Chem. Soc., Faraday Trans.* **1992**, *88*, 2595.
(11) Howells, B. D.; McCombie, J.; Palmer, T. F.; Simons, J. P.; Walters, A. *J. Chem. Soc., Faraday Trans.* **1992**, *88*, 2603.
(12) Fernandez, J. A.; Longarte, A.; Unamuno, I.; Castaño, F. *J. Chem. Phys.* **2000**, *113*, 8531.
(13) Longarte, A.; Fernandez, J. A.; Unamuno, I.; Castaño, F. *Chem. Phys.* **2000**, *260*, 83.
(14) Aguado, E.; Longarte, A.; Alejandro, E.; Fernandez, J. A.; Castaño, F. *J. Phys. Chem. A* **2006**, *110*, 6010.
(15) Pereira, R.; Alava, I.; Castaño, F. *J. Chem. Soc., Faraday Trans.* **1994**, *90*, 2443.
(16) Longarte, A.; Redondo, C.; Fernandez, J. A.; Castano, F. *J. Chem. Phys.* **2005**, *122*, 164304.
(17) Satta, M.; Latini, A.; Piccirillo, S.; Di Palma, T. M.; Scuderi, D.; Speranza, M.; Giardini, A. *Chem. Phys. Lett.* **2000**, *316*, 94.
(18) Haines, S. R.; Dessent, C. E. H.; Muller-Dethlefs, K. *J. Chem. Phys.* **1999**, *111*, 1947.
(19) Wickleder, C.; Henseler, D.; Leutwyler, S. *J. Chem. Phys.* **2002**, *116*, 1850.
(20) Wickleder, C.; Droz, T.; Burgi, T.; Leutwyler, S. *Chem. Phys. Lett.* **1997**, *264*, 257.
(21) Cerny, J.; Hobza, P. *Phys. Chem. Chem. Phys.* **2007**, *9*, 5291.
(22) Boys, S. F.; Bernardi, F. *Mol. Phys.* **1970**, *19*, 553.
(23) Gu, Q.; Knee, J. L. *J. Chem. Phys.* **2008**, *128*, 064311.
(24) C.Fajin, J. L.; Capelo, S. B.; Fernandez, B.; Felker, P. M. *J. Phys. Chem. A* **2007**, *111*, 7876.
(25) Ishiuchi, S. I.; Tsuchida, Y.; Dopfer, O.; Muller-Dethlefs, K.; Fujii, M. *J. Phys. Chem. A* **2007**, *111*, 7569.

JP808723R